RSC Applied Interfaces

ROYAL SOCIETY OF CHEMISTRY

PAPER

View Article Online
View Journal | View Issue

Cite this: *RSC Appl. Interfaces*, 2026, 3, 564

Utilizing a Pickering emulsion for the Suzuki–Miyaura coupling with an amine-coordinated Pd catalyst

Mingshuang Li, [ab] Junhao Huang,[a] Xing-Bao Wang[b] and Yuanyuan Shan*[a]

Received 21st November 2025,
Accepted 29th January 2026

DOI: 10.1039/d5lf00367a

rsc.li/RSCApplInter

The Suzuki–Miyaura coupling reaction catalyzed by transition metals and their complexes for the construction of C–C bonds has been widely used in many fields. However, there have been problems such as difficulty in recycling homogeneous catalysts and low transfer efficiency of heterogeneous catalysts in reactions. To address above problems, an amine-coordinated Pd catalyst (GO-DAP-$PdCl_2$) was prepared by coordinating $PdCl_2$ on graphene oxide (GO) with a solid-loaded amine ligand (2,6-diaminopyridine, DAP) on the surface. Among which the amphiphilic Pickering emulsion catalyst (GO-DAP) could form stable O/W emulsions, where the hydrophilic GO sheets and hydrophobic DAP moieties were anchored at the oil–water interface to provide a high interfacial area for the reaction, and significantly reduce the mass-transfer resistance between the two phases. In the Suzuki–Miyaura coupling reaction, the coordination Pd-based Pickering emulsion catalyst (GO-DAP-$PdCl_2$) showed excellent catalytic performance; the conversion rate of iodobenzene reaches up to 95%, the TOF reaches up to 14 100 h^{-1}, the conversion still reaches up to 85% after 6 cycles, and the catalyst also exhibits good substrate suitability.

Introduction

The Suzuki–Miyaura (SM) coupling reaction, first reported by the Japanese chemists Suzuki and Miyaura in 1979, is a classic method for constructing C–C bonds in organic synthesis.[1] Owing to its high efficiency and broad substrate scope, this reaction has become a cornerstone in modern synthetic chemistry.[2,3] The catalytic mechanism involves three fundamental steps: oxidative addition, transmetalation, and reductive elimination.[4] Among these, oxidative addition and transmetalation are recognized as the rate-determining steps.[5,6] Early studies primarily focused on homogeneous catalytic systems, which exhibit high activity but suffer from drawbacks such as difficult catalyst separation and recovery, poor recycling stability, and residual metal contamination.[7–9] These limitations have significantly restricted their application in large-scale industrial production. Although heterogeneous catalytic systems can alleviate the issue of catalyst recovery, they still face challenges such as low mass-transfer efficiency and excessive consumption of organic solvents, which contradict the principles of green chemistry.[10–12] Therefore, how to maintain high catalytic activity while improving catalyst stability and recyclability, and simultaneously reducing mass-transfer resistance in multiphase systems, remains a key challenge in this field.

To address these challenges, coordination metal catalysis has emerged as a promising strategy. As an important branch of metal catalysis, this strategy creates highly stable active sites by directional coordination between ligands and metal centers, providing well-defined spatial and electronic environments. Such design allows for precise control of reaction pathways while effectively preventing metal leaching and aggregation.[13–16] For example, Tang *et al.*[17] reported the self-assembly of Cu-X MOFs (X = Cl, Br, I) from copper ions, halide ions, and 4,4′-bipyridine, where halide coordination finely tuned the geometry and electronic structure of the copper active sites, thereby regulating enzyme-like activity. In these systems, active centers are formed through coordination bonds between metal atoms and specific ligands, such as phosphines or N-heterocyclic carbenes.[18–21] Among these, amine ligands have received particular attention due to their diverse coordination modes and ease of functionalization.[22] Therefore, this study employed amine ligands to stabilize the palladium active sites. However, significant mass-transfer resistance remains at the interfaces in multiphase coordination catalytic systems. This resistance limits the overall catalytic efficiency.

In recent years, Pickering emulsion interfacial catalysis has attracted increasing attention owing to its unique interfacial stabilization mechanism and superior mass-transfer

[a] *Institute of New Carbon Materials, College of Materials Science and Engineering, Taiyuan University of Technology, Taiyuan 030024, China.*
E-mail: shanyuanyuan@tyut.edu.cn
[b] *State Key Laboratory of Clean and Efficient Coal Utilization, Taiyuan University of Technology, Taiyuan 030024, China*

efficiency.[23,24] Unlike traditional surfactants, Pickering emulsions are stabilized by solid particles (*e.g.*, nanoparticles or two-dimensional materials) adsorbed at oil–water interfaces.[25,26] These particles not only reduce interfacial tension, but also form dense physical barriers, effectively preventing droplet coalescence and thus ensuring emulsion stability.[27,28] As a result, each droplet can act as an independent microreactor, significantly expanding the interfacial area for biphasic reactions, shortening substrate diffusion pathways, and reducing mass-transfer resistance.[29–31] For instance, Gao *et al.*[32] prepared controllable Pickering emulsions *via* sulfobutylation modification of lignin, followed by the *in situ* deposition of Pd nanoparticles. This catalyst achieved complete conversion of nitrobenzene to aniline within 3 h at room temperature. These findings demonstrate that Pickering emulsion catalysis offers significant advantages in enhancing interfacial mass-transfer efficiency and overall catalytic performance.[33]

In this work, coordination metal catalysis is combined with Pickering emulsion interfacial catalysis to develop a stable O/W Pickering emulsion catalytic system. Amine-coordinated $PdCl_2$ active sites are immobilised on the emulsifier surface, resulting in the stable confinement of catalytically active Pd species at the oil–water interface. This interfacial localisation markedly increases the available reaction interface and reduces mass-transfer limitations. The synergistic effects arising from interfacial confinement and spatially differentiated microenvironments facilitate the activation of both arylboronic acids and aryl halides, thereby promoting the key elementary steps of the Suzuki–Miyaura coupling reaction. In addition, the interfacial architecture effectively suppresses Pd aggregation and leaching, leading to enhanced catalytic stability and recyclability. Furthermore, the use of water as the continuous phase reduces the consumption of organic solvents and enables straightforward catalyst recovery, highlighting the potential of this system for green and sustainable catalysis.

Experimental

Chemicals and reagents

Palladium chloride ($PdCl_2$, 99.0% purity), iodobenzene (99.0% purity), chlorobenzene (99.0% purity), bromobenzene (99.0% purity), phenylboronic acid (>98.0% purity), 2-iodoanisole (>98.0% purity), 3-iodoanisole (>98.0% purity), 4-iodoanisole (97.0% purity), 4-iodotoluene (>98.0% purity), 4-nitroiodobenzene (99.0% purity), and various bases (sodium carbonate, 98.0% purity; potassium carbonate, >99.5% purity; cesium carbonate, 99.9% purity; potassium hydroxide, >98.0% purity; potassium phosphate, analytical grade; sodium hydroxide, >96.0% purity; sodium bicarbonate, >98.0% purity) were purchased from Shanghai Adamas Reagent Co. Ltd. Graphite, potassium permanganate (>99.0% purity), sodium nitrate (analytical grade), concentrated sulfuric acid (>95.0% purity), and toluene (analytical grade) were obtained from Sinopharm Chemical Reagent Co. Ethanol (>99.7% purity) was obtained from Tianjin Zhiyuan Chemical Reagent Co. 2,6-Diaminopyridine (97.0% purity) was purchased from Shanghai Aladdin Biotechnology Co. Concentrated hydrochloric acid (analytical grade) was obtained from Chengdu Cologne Chemical Co. Hydrogen peroxide (30% purity) was supplied by Tianjin Obokai Chemical Co. All chemicals were of the highest purity available and were used as received without further purification.

Characterization

Transmission electron microscopy (TEM) images were obtained using a JEOL JEM-1400 microscope. The sample powder was ultrasonically dispersed in ethanol to prepare a suspension, and a drop of the suspension was deposited onto a copper grid. After ethanol evaporation, the grid was placed in a TEM sample chamber for morphological observation and imaging. The surface morphology and particle size of the material were characterized by scanning electron microscopy (SEM, JSM-7900F). Powder X-ray diffraction (XRD) patterns were recorded on a LabX XRD-6100 diffractometer under the conditions of a 2θ range from 5° to 80° with a scanning rate of 4° min^{-1}, using Cu Kα radiation (λ = 1.5418 Å). Fourier transform infrared (FT-IR) spectra were collected on a Thermo Fisher Nicolet™ IS50 spectrometer. The samples were prepared by the KBr pellet method, in which the sample and KBr were thoroughly mixed at a mass ratio of 1 : 100, pressed into transparent pellets under 15 MPa to ensure high signal transmittance, and measured in the wavenumber range of 400–4000 cm^{-1}. X-ray photoelectron spectroscopy (XPS) was performed using a Kratos AXIS Supra spectrometer with a maximum power of 72 W and an energy scanning range of 0–1500 eV to analyze the surface chemical composition of the samples. Raman spectra were recorded using a Thermo Scientific DXR2 Raman spectrometer to analyze the characteristic carbon peaks of the material, with a spectral range of 50–9000 cm^{-1}, using a 50× long-focus objective lens. After setting the spectral range and other parameters, spectra were collected accordingly. The emulsion type was characterized using a THUNDER Imager Tissue fluorescence microscope. The water contact angle of the material was measured using a SINDIN CSCDIC-100 instrument. The metal dispersion of palladium was determined by CO-Pulse Chemisorption using an AutoChem II 2920 instrument. The sample was first pretreated under a H_2 atmosphere at 200 °C for 2 h to remove surface impurities, followed by cooling to 50 °C. Subsequently, successive CO pulses were introduced into the system until saturation of the adsorption signal was achieved.

Preparation of GO-DAP

In this study, GO was synthesized using a modified Hummers' method,[34] with the detailed procedure provided in the SI. The preparation of GO-DAP was as follows: 100 mg GO and 320 mg NaOH were dispersed in 35 mL of deionized water. The mixture was stirred for 10 min and then sonicated for 30 min. Subsequently, a predetermined amount of DAP

was added, followed by an additional 10 min of sonication and 3 h of stirring in a water bath at 70 °C. After completion of the reaction and cooling to room temperature, GO-DAP was washed with deionized water until neutral, freeze-dried, and stored for further use.

Preparation of GO-DAP-$PdCl_2$

In brief, 30 mg GO-DAP was dispersed in 80 mL of ethanol and sonicated for 1 h. Subsequently, 635 μL of $PdCl_2$ hydrochloric acid aqueous solution (6.7 mg mL^{-1}) was added, and the mixture was stirred at room temperature for 24 h. After completion of the reaction, the product was washed three times with ethanol and deionized water, respectively, followed by freeze-drying to obtain GO-DAP-$PdCl_2$. The preparation process of GO-DAP-$PdCl_2$ is illustrated in Fig. 1.

Preparation of the Pickering emulsion

A certain amount of GO-DAP was dispersed in deionized water in a 15 mL glass vial and sonicated for 1 h. After GO-DAP was evenly dispersed in water, toluene was added to it, and emulsified with a high-speed shear for 2 min (10 000 r min^{-1}). The mixture was allowed to rest for 1 h before a microscope photograph was taken.

Catalytic experiment

In the SM coupling reaction, 6 mg of GO-DAP-$PdCl_2$ and 2 mmol of K_2CO_3 were added to a reaction vial containing 8 mL of deionized water. The mixture was sonicated for 1 h to ensure uniform dispersion of all components. Subsequently, 1 mmol of iodobenzene and 2 mmol of phenylboronic acid were introduced into the reaction mixture to form an emulsion, which was then employed for the SM coupling. Upon completion of the reaction, the products were extracted with toluene and analyzed by gas chromatography (GA-2009). The TOF value is determined based on the conversion rate achieved after 10 min of reaction and calculated using eqn (1).

$$\mathrm{TOF} = \frac{n}{n_{\mathrm{cat}} \times D \times t} \quad (1)$$

In eqn (1), n represents the amount of substance of the reaction product formed within a specific reaction time, n_{cat} denotes the total amount of substance of palladium in the reaction system, and D is the metal dispersion degree of Pd. Based on the 1 : 1 specific chemisorption between Pd and CO, the dispersion degree was calculated as the ratio of surface-accessible Pd atoms to the total Pd atoms in the catalyst, and t represents the reaction duration.

Results and discussion

Morphology and structure

SEM and TEM analyses were performed to investigate the micromorphology of the samples. As shown in the SEM images (Fig. 2a–c), GO exhibits a smooth lamellar structure. Upon grafting amine ligands onto GO, pronounced wrinkles appeared on the surface, while the overall layered morphology was largely preserved. After $PdCl_2$ adsorption, the wrinkled lamellae exhibited partial aggregation. Further analysis of the TEM images (Fig. 2d–f) reveals that GO displays a translucent lamellar structure with slight wrinkles and folds, which can be attributed to its inherent flexibility and the abundance of oxygen-containing functional groups. Compared with GO, the surface of GO-DAP became rougher, likely due to DAP modification introducing additional functional groups onto the GO surface. Following $PdCl_2$ modification, the surface of GO-DAP-$PdCl_2$ becomes rougher. However, no distinct solid particles are visible. This suggests that $PdCl_2$ is mainly present on the material surface in ionic form. Moreover, SEM-EDS elemental mapping of GO-DAP-$PdCl_2$ (Fig. 2g) confirms that C, O, N, Pd, and Cl are uniformly distributed across the GO surface. Collectively, these results demonstrate that DAP was successfully grafted onto GO and GO-DAP has successfully captured Pd^{II}.

The structures of the samples were characterized by XRD. As shown in Fig. 3a, GO exhibits a characteristic diffraction

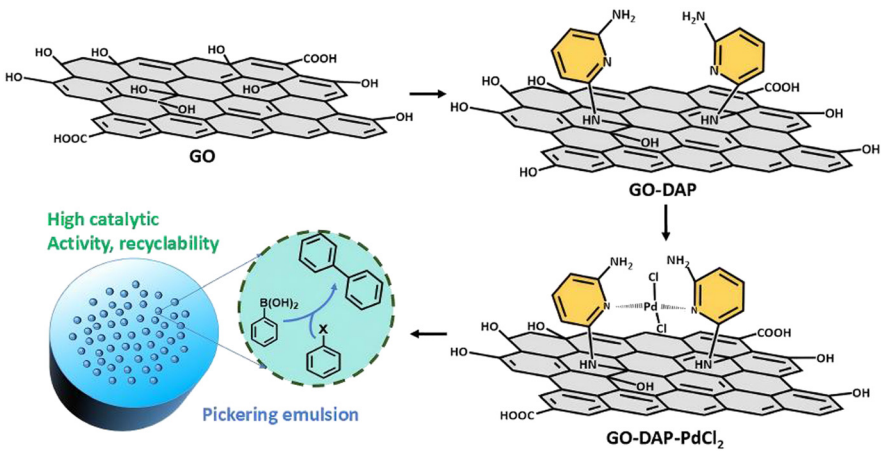

Fig. 1 Schematic illustration of Pickering catalyst GO-DAP-$PdCl_2$ synthesis for the configured Suzuki–Miyaura coupling reaction under a droplet reactor.

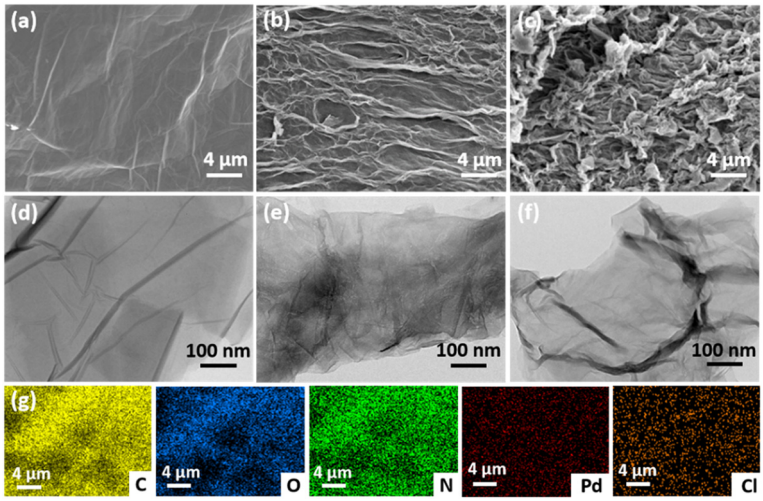

Fig. 2 SEM images of GO (a), GO-DAP (b) and GO-DAP-$PdCl_2$ (c). TEM images of GO (d), GO-DAP (e) and GO-DAP-$PdCl_2$ (f). SEM-EDS elemental mappings of GO-DAP-$PdCl_2$ (g).

peak at 2θ = 12.9°, corresponding to the (001) crystal plane,[35] which shifts to 11.7° after DAP modification. According to Bragg's law, the decrease in diffraction angle indicates an increase in interlayer spacing.[36] Therefore, it is speculated that DAP reacts with oxygen-containing functional groups on the GO surface. This reaction reduces interlayer interactions. As a result, the interlayer spacing in GO-DAP increases. A comparison of the XRD patterns of GO-DAP and GO-DAP-$PdCl_2$ reveals no significant difference; this may be because the increased structural disorder of GO-DAP diminishes the effect of $PdCl_2$ on its structure.

The structural properties of the materials and the effects of functional modification were further analyzed by Raman spectroscopy (Fig. 3b). The spectra of GO, GO-DAP, and GO-DAP-$PdCl_2$ show two characteristic peaks at 1355 and 1592 cm^{-1}. These correspond to the D band and G band, respectively. The D band relates to structural defects. The G band represents the in-plane vibration of sp^2 carbon. The intensity ratio (I_D/I_G) is commonly used to evaluate the defect density of graphene-based materials, with a higher ratio indicating more structural defects and greater disorder.[37] Based on the spectra, the I_D/I_G ratio of GO is 0.80, which increases to 0.91 after DAP modification. This suggests that the sp^2 carbon network of GO is partially disrupted and new sp^3-hybridized carbon is introduced.[38] Combined with the XRD results, these findings indicate that DAP reacts with some oxygen-containing functional groups on the GO surface, thereby increasing atomic disorder after amine modification. Upon the addition of $PdCl_2$, the I_D/I_G ratio further rises to 0.94. This increase likely results from the formation of coordination bonds between Pd^{II} ions and nitrogen atoms in the amino groups. Such bonding induces local structural distortion on the GO surface. Consequently, the defect density increases.

Surface chemistry

To further elucidate the bonding interaction between GO and DAP, FT-IR and XPS analyses were conducted. As shown in the FT-IR spectra (Fig. 4a), compared with GO, GO-DAP exhibits a new vibration peak at 1155 cm^{-1} corresponding to the C–N bond. Meanwhile, the stretching and bending vibrations of C–O–C at 1055 cm^{-1} are significantly weakened, and the intensity of the C–O stretching vibration at 1726 cm^{-1} also decreases. Furthermore, the XPS full spectra (Fig. 4b) show that GO-DAP displays a characteristic N 1s peak at 400.3 eV, accompanied by a marked reduction in the O 1s

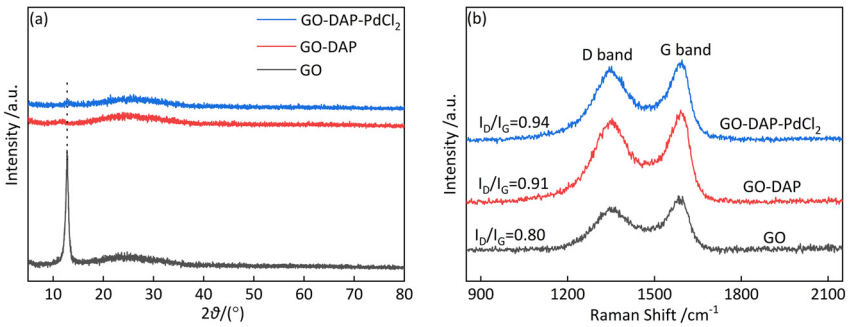

Fig. 3 XRD spectra (a) and Raman spectra (b) of GO, GO-DAP and GO-DAP-$PdCl_2$.

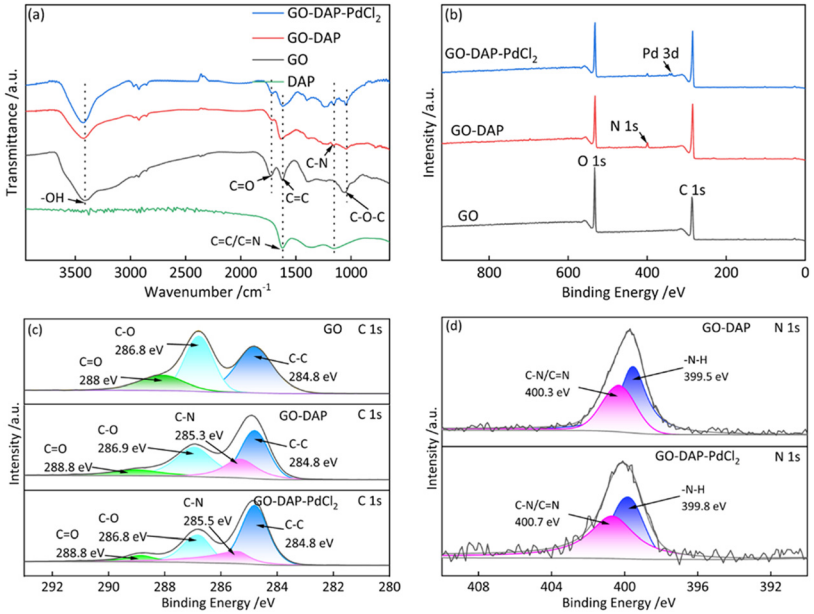

Fig. 4 FT-IR spectra of GO, GO-DAP, DAP and GO-DAP-$PdCl_2$ (a). XPS full spectra (b) and C 1s high-resolution XPS spectra (c) of GO, GO-DAP, and GO-DAP-$PdCl_2$. N 1s high-resolution XPS spectra of GO-DAP and GO-DAP-$PdCl_2$ (d).

peak intensity. These results indicate that GO-DAP is formed through chemical reactions between the C–N bonds of DAP and the C–O–C or C–O bonds of GO. Moreover, the high-resolution C 1s spectrum of GO-DAP (Fig. 4c) reveals a new signal at 285.3 eV corresponding to the C–N bond. Taken together, the FT-IR and XPS results suggest that GO-DAP is generated *via* a ring-opening reaction between the C–N bonds of DAP and the C–O bonds of GO.

To determine the chemical state of Pd on GO-DAP, the XPS spectrum of GO-DAP-$PdCl_2$ was analyzed. As shown in Fig. S1, the Pd $3d_{5/2}$ and $3d_{3/2}$ peaks appear at 337.5 eV and 342.8 eV, respectively, which are characteristic of Pd^{II}. This indicates that Pd is present in the form of Pd^{II} in GO-DAP-$PdCl_2$. In addition, a characteristic Cl peak is observed in the XPS full spectra, and the Cl 2p spectrum (Fig. S2) exhibits a characteristic absorption peak at approximately 199.7 eV, confirming that Pd exists as $PdCl_2$ on the surface of GO-DAP. Furthermore, the high-resolution N 1s spectra of GO-DAP and GO-DAP-$PdCl_2$ (Fig. 4d) reveal a shift in the binding energy of the C–N bond from 400.3 eV to 400.7 eV. This shift can be attributed to the coordination interaction between Pd^{II} and the nitrogen atoms, which decreases the electron density around N and consequently leads to a higher binding energy.[39]

Emulsion optimization

According to desorption energy theory, the formation of Pickering emulsions is governed by the wettability of solid particle surfaces, with the three-phase contact angle serving as a key evaluation parameter.[40] In this study, the water contact angles of GO, GO-DAP, and GO-DAP-$PdCl_2$ were measured (Fig. S3). The results demonstrated that both GO-DAP and GO-DAP-$PdCl_2$ particles exhibited suitable amphiphilic properties for stabilizing emulsions.

The oil-to-water volume ratio plays a crucial role in the formation and functional performance of emulsions, as it affects the interfacial force balance, spatial distribution of the dispersed phase, and the adsorption efficiency of emulsifiers.[41] To investigate this effect, Pickering emulsions were prepared using toluene as the oil phase with oil-to-water ratios of 1 : 7, 1 : 10, 1 : 14, 1 : 23, and 1 : 70. As shown in Fig. 5a–e, the average droplet size gradually decreased with decreasing oil-to-water ratio. Notably, even at an oil-to-water ratio as low as 1 : 70, a stable emulsion with uniform droplet distribution and an average diameter of approximately 20 μm was still obtained. Smaller droplets provide a larger oil–water interfacial area, increasing the probability of contact between the reactants and the catalytic active sites, thereby accelerating the mass transfer rate of hydrophobic substrates and enhancing the overall reaction rate. Subsequently, the oil phase was fluorescently stained to further confirm that the emulsion was of the O/W type (Fig. 5f). Furthermore, the catalyst was fluorescently labeled with fluorescein isothiocyanate (FITC) and the Pickering emulsion was examined using confocal laser scanning microscopy (CLSM). The CLSM image (Fig. 5g) indicates that the catalyst is predominantly located at the oil–water interface, consistent with the proposed interfacial catalysis mechanism.

In the SM coupling reaction, the concentration of base plays a crucial role in determining reaction efficiency and selectivity. An appropriate base concentration facilitates the deprotonation of phenylboronic acid, leading to the formation of more reactive boronate species and thereby accelerating the transmetalation step in the catalytic cycle.[42] In Pickering emulsion systems, variations in base concentration may also influence emulsion stability and interfacial behavior. In this

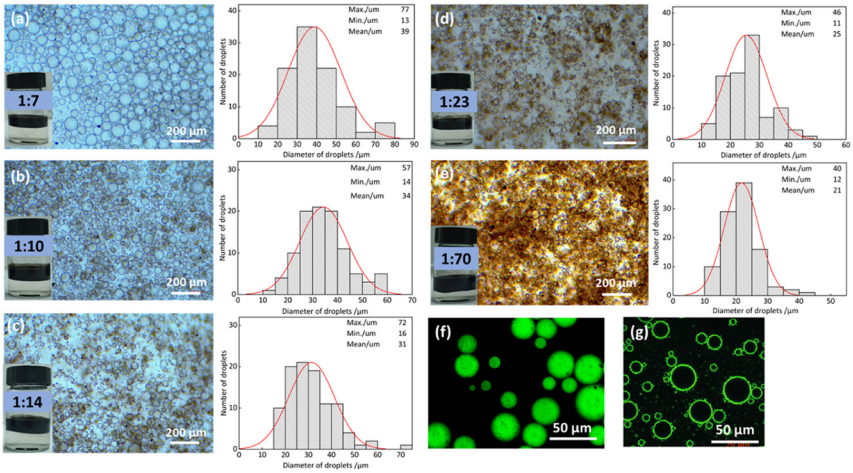

Fig. 5 Effects of emulsion and histograms of particle size distribution at different oil–water volume ratios (a–e). Fluorescence microscope image of the emulsion (f). Confocal laser scanning microscopy (CLSM) image of the Pickering emulsion stabilized by the FITC-labeled catalyst (g).

study, the effect of different base amounts on the formation of Pickering emulsions was investigated. As shown in Fig. S4, when the amount of base increased from 2 to 10 mmol, the average droplet size remained approximately 50 μm with a uniform size distribution. This result indicates that the Pickering emulsions stabilized by GO-DAP maintain excellent stability even under highly basic conditions. This stability can be attributed to the strong interfacial adsorption of GO-DAP particles, which helps maintain the balance of interfacial tension even in the presence of excess hydroxide ions. Moreover, the protonation–deprotonation equilibrium of amino groups under basic conditions enhances electrostatic repulsion between particles, effectively preventing aggregation and preserving the structural integrity of the emulsion droplets.

In addition to the effects of the oil–water ratio and alkali concentration, the stability of Pickering emulsions under practical reaction conditions, including elevated temperature and mechanical stirring, is essential for maintaining reliable catalytic performance. Accordingly, systematic experiments were performed to evaluate the thermal stability of the emulsion and its structural integrity under continuous agitation.

To probe the emulsion stability during the reaction, the droplet size of the GO-DAP-$PdCl_2$-stabilized Pickering emulsion was monitored at different time intervals. As shown in Fig. S5, the emulsion remained stable throughout the reaction. After 3 h, the average droplet diameter increased slightly from the initial value of approximately 25 μm to about 37 μm, while no obvious droplet coalescence, phase separation, or demulsification was observed. These results indicate that the Pickering emulsion retains good structural stability under the reaction conditions. Notably, heating at 85 °C did not disrupt the emulsion, which can be attributed to the suitable amphiphilicity of the GO-DAP particles. Their strong adsorption at the oil–water interface, associated with an adsorption energy substantially higher than the thermal energy at 85 °C, effectively suppresses particle desorption and emulsion destabilization. At the same time, under continuous stirring at 500 rpm, the Pickering emulsion interface remained intact, and a more homogeneous droplet dispersion was observed. This behavior can be ascribed to the cooperative contribution of multiple interactions among the GO-DAP particles, including electrostatic repulsion between protonated amine groups and van der Waals interactions between GO sheets, which together enhance the mechanical robustness of the interfacial film. As a result, the emulsion withstands shear forces without noticeable structural degradation. Meanwhile, stirring facilitates mass transfer of reactants to the interfacial catalytic sites without inducing catalyst desorption, thereby contributing to improved reaction efficiency.[43,44]

Overall, these results demonstrate that the GO-DAP-$PdCl_2$-stabilized Pickering emulsion exhibits good thermal and mechanical stability under the applied reaction conditions. The preservation of emulsion integrity at elevated temperature and under continuous stirring ensures the sustained availability of the interfacial catalytic environment, which is closely associated with the high catalytic activity and recyclability of the system.

Reaction optimization

In this study, a Pickering emulsion system was constructed using the substrate as the oil phase, and the optimal reaction conditions were systematically investigated. As shown in Fig. 6a, the catalytic yield increased progressively with reaction time and reached a plateau after 3 h, which was identified as the optimal reaction time. Fig. 6b shows the effect of reaction temperature; as the temperature increased from 25 to 95 °C, the conversion rate rose sharply from 4% to 99%, indicating that elevated temperature significantly accelerated the coupling reaction. This enhancement can be mainly attributed to the improved solubility and diffusivity of the reactants in the biphasic medium at higher temperatures. However, excessively high temperatures may lead to water evaporation and disruption of

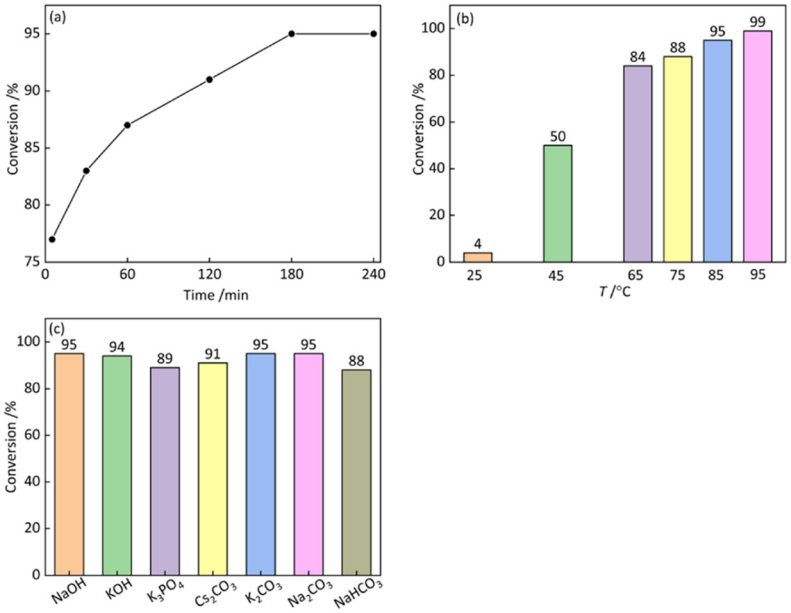

Fig. 6 Effects of (a) reaction time, (b) reaction temperature and (c) the type of base on the conversion of the Suzuki–Miyaura cross-coupling reactions.

emulsion droplets, resulting in catalyst aggregation and the loss of interfacial active sites. Therefore, 85 °C was selected as the optimal reaction temperature to balance catalytic efficiency and emulsion stability. In addition, the effect of different base types on the reaction was evaluated. As shown in Fig. 6c, all tested bases afforded high conversion rates, suggesting good adaptability of the catalytic system. Among them, K_2CO_3 exhibited the highest catalytic performance, which may be attributed to the relatively large ionic radius of K^+, facilitating easier ion dissociation and thereby enhancing the overall reaction activity. In summary, the optimal reaction conditions were determined to be a temperature of 85 °C, a reaction time of 3 h, and K_2CO_3 as the base. Under these conditions, the system achieved both high catalytic conversion and excellent emulsion stability.

Catalytic performance

To evaluate the high activity of GO-DAP-$PdCl_2$, the reaction conversion rate was investigated under the condition of increased substrate amount. As shown in Fig. 7a, when the substrate amount was enlarged by 10 times, the reaction conversion rate decreased from 95% to 90%, with only a 5% activity decay rate. As shown in Fig. 7b, the conversion rate and TOF value at 5 min of reaction were calculated under different substrate amounts, with the TOF reaching as high as 14 100 h^{-1}. Combined with the previous emulsion particle size analysis, the smaller droplets provide a larger interfacial area, exposing more Pd active sites at the reaction interface, thus achieving the high catalytic activity of GO-DAP-$PdCl_2$.

To further highlight the unique advantages of the Pickering emulsion platform, three catalytic systems were compared under strictly identical conditions, including catalyst type, Pd loading, substrate ratio, temperature, and reaction time: a non-emulsified biphasic system, a conventional heterogeneous system (toluene as the sole solvent), and the Pickering emulsion system developed in this work. As shown in Fig. 8a, the non-emulsified biphasic system and the heterogeneous system exhibited limited conversions of 45% and 63%,

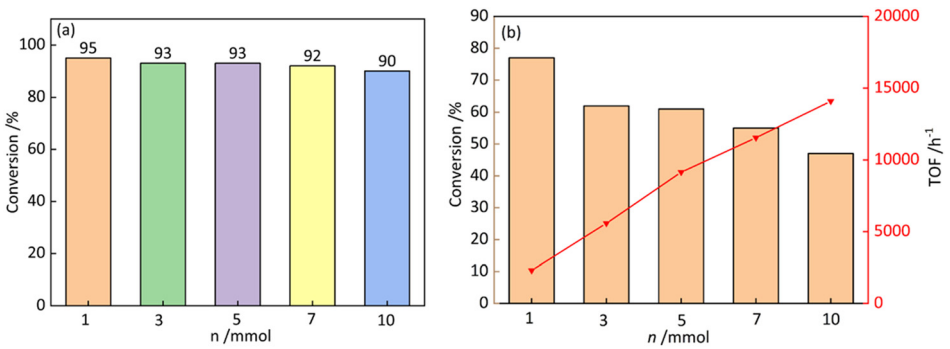

Fig. 7 Effects of the reaction substrate amount on the Suzuki–Miyaura cross-coupling reaction at 3 h (a) and 5 min (b).

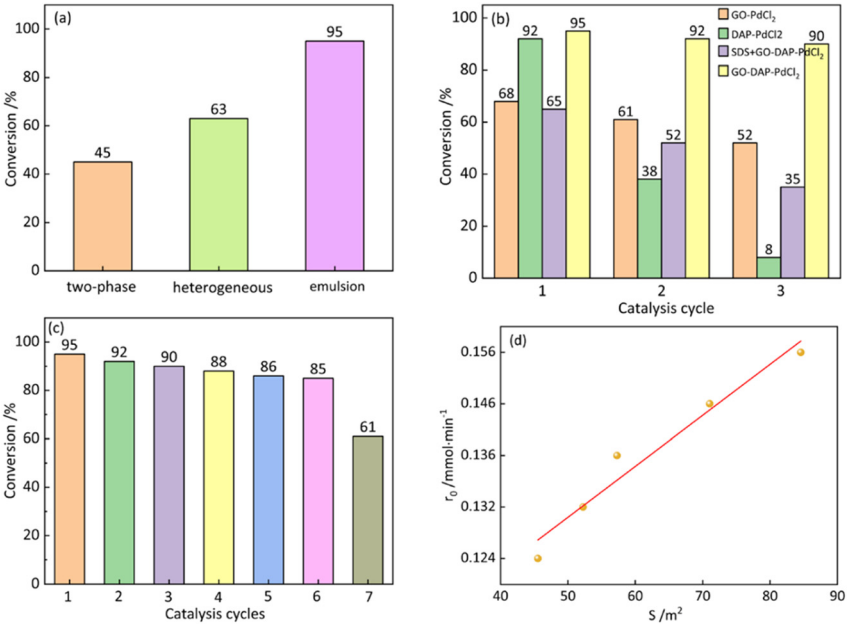

Fig. 8 Conversion of the SM coupling reaction under different reaction systems (a). Catalytic performance and three-cycle stability test of different catalyst systems (b). Cycling performance of GO-DAP-$PdCl_2$ in the Suzuki–Miyaura cross-coupling reaction (c). Dependence of the initial reaction rate (r_0) on the total interfacial area (S) in the GO-DAP-$PdCl_2$ Pickering emulsion system (d).

respectively, due to mass transfer restrictions arising from insufficient interfacial contact. In contrast, the Pickering emulsion system, in which the catalyst simultaneously acts as an emulsifier, generated an enlarged interfacial area, thereby shortening the diffusion path of reactants and increasing the conversion to 95%. These results demonstrate that the Pickering emulsion platform effectively addresses the mass transfer limitations inherent to biphasic catalysis.

To further investigate the synergistic mechanism of this system, we conducted a series of performance experiments with different catalytic systems to examine the individual contributions of amine coordination and the Pickering emulsion interface (Fig. 8b). The GO-$PdCl_2$ without DAP exhibits significantly lower conversion (58%) and poorer recyclability, confirming that amine coordination stabilizes Pd active sites, making them more stable, while also imparting amphiphilicity to GO, which enables the formation of a stable Pickering emulsion. Furthermore, the homogeneous DAP-$PdCl_2$ complex achieved a high initial conversion (92%), but its recycling efficiency was very low, indicating that while DAP enhances Pd activity, the absence of a Pickering emulsion limits mass transfer and catalyst recovery. Finally, we formed an emulsion using the conventional surfactant (SDS) and then added the GO-DAP-$PdCl_2$ catalyst. The conversion was still relatively low (65%), and we observed rapid droplet coalescence, with the emulsion failing to remain stable (Fig. S6), which indirectly demonstrates the superior stability of Pickering emulsions in facilitating reactions and maintaining high catalytic performance. In summary, the high catalytic performance of the GO-DAP-$PdCl_2$ system arises from the synergistic effect between amine coordination and the Pickering interface: amine coordination stabilizes the active centers through electronic regulation and imparts amphiphilicity to the support, while the Pickering interface enhances mass transfer efficiency and facilitates the efficient recovery of the catalyst.

It is noteworthy that the GO-DAP-$PdCl_2$ system not only exhibits high activity in single-use reactions but also demonstrates excellent stability during practical recycling. As shown in Fig. 8c, the conversion rate decreased slightly from 95% to 85% after six reaction cycles. This result demonstrates that GO-DAP-$PdCl_2$ maintains high catalytic activity after repeated use and exhibits excellent recyclability. To investigate the cause of the activity decline, the catalysts subjected to different numbers of cycles were systematically characterized in terms of their microstructure and chemical states. TEM images of the catalyst after different numbers of cycles were obtained (Fig. S7). The images revealed the formation of numerous solid particles on the catalyst surface after multiple reactions. This phenomenon can be attributed to the reduction of Pd^{II} to Pd^0 during the reaction, accompanied by an increase in the average size of Pd nanoparticles. After six cycles, Pd^0 agglomeration became evident, leading to a reduction in accessible active sites and, consequently, a decline in catalytic efficiency.

To further clarify the valence-state evolution, XPS measurements were performed on the catalyst after six cycles. As shown in Fig. S8, a portion of Pd^{2+} was indeed reduced to Pd^0 after 6 recycles. This result is consistent with the particle aggregation observed in the TEM images, collectively indicating that the slight loss of catalytic activity primarily originates from the reduction and aggregation of Pd active species, which results in the depletion of available active sites.

The substrate scope of the SM coupling reaction catalyzed by GO-DAP-$PdCl_2$ was examined under the optimized reaction conditions. To assess the influence of electronic and steric

effects, haloarenes bearing different substituents were selected for coupling with phenylboronic acid. As summarized in Table S1, *ortho*- and *meta*-substitutions had little impact on the reaction yield, whereas *para*-substitution resulted in reduced product conversion. This decrease is likely due to the physical state of the *para*-substituted substrate, 4-methoxyiodobenzene, which is solid under the reaction conditions and therefore unable to form a stable emulsion system. A comparison of 4-nitroiodobenzene and 4-iodotoluene revealed that electron-withdrawing substituents, such as the nitro group, significantly promote the reaction. In contrast, substrates such as bromobenzene and chlorobenzene exhibited much lower reactivity because of the higher bond dissociation energies of the C–Br and C–Cl bonds. During the oxidative addition step, these stronger C–X bonds are less readily activated, resulting in diminished catalytic activity.[45] Overall, the GO-DAP-$PdCl_2$ catalyst demonstrates excellent substrate tolerance in SM coupling reactions.

Mechanistic insights

Although the elementary steps and general principles of the SM coupling reaction have been extensively documented,[46,47] the kinetic behavior of the present system is fundamentally altered by the combined effects of amine coordination and Pickering interfacial confinement. To elucidate the individual roles of these two factors, initial reaction rate measurements were conducted at short reaction times ($\leq$5 min), where product accumulation and interfacial evolution effects are minimized; the corresponding calculation procedures are provided in the SI.[48,49] As summarized in Table S2, the GO-$PdCl_2$ system exhibits a markedly lower reaction rate under identical conditions, indicating reduced intrinsic activity of the Pd center in the absence of amine coordination. This behavior can be attributed to an unfavorable electronic environment and decreased stability of the Pd species. In contrast, the homogeneous DAP-$PdCl_2$ complex shows a relatively higher initial activity, demonstrating that amine coordination intrinsically enhances Pd-catalyzed coupling. However, its poor recyclability highlights that ligand coordination alone is insufficient to overcome the mass-transfer limitations inherent to biphasic reaction systems. Notably, the highest initial reaction rate is observed for the GO-DAP-$PdCl_2$ Pickering emulsion, in which amine-coordinated Pd sites are immobilized at the oil–water interface. This interfacial configuration allows hydrophobic aryl halides to approach the active sites from the oil phase while hydrophilic boronate species simultaneously access them from the aqueous phase.

XPS further provides direct evidence for electronic interactions between the amine ligand and the Pd center. As shown in Fig. 4d, the N 1s binding energy shifts from 400.3 eV in GO-DAP to 400.7 eV upon Pd coordination, indicating electron donation from the amine nitrogen atoms to the Pd center. Acting as a σ-donor ligand, the DAP increases the electron density at Pd,[50,51] thereby facilitating oxidative addition of aryl halides and promoting the subsequent transmetalation step.

Based on the above kinetic and electronic-structure analyses, a corresponding reaction mechanism is proposed in Fig. S9. The catalytic process follows a classical Pd^{2+}/Pd^{4+} cycle, in which amine coordination stabilizes high-valent Pd intermediates, suppresses catalyst deactivation, and electronically promotes the key steps of oxidative addition, transmetalation, and reductive elimination.[52–54] Furthermore, systematic variation of the oil–water ratio was performed to probe the influence of the interfacial area on reaction kinetics. The results (Fig. 8d) reveal a strong correlation between the initial reaction rate and the interfacial area, indirectly indicating that catalytic conversion predominantly occurs at the Pickering emulsion interface rather than within the bulk droplets. Combined with the CLSM image (Fig. 5g), which clearly shows the pronounced enrichment of the catalyst at the oil–water interface, this spatial localisation provides direct morphological evidence for the interfacial confinement catalytic mechanism. Taken together, these results demonstrate that the synergistic effects of interfacial confinement and amine coordination stabilisation collectively govern the efficient Suzuki–Miyaura coupling reaction.

Conclusions

A novel amine-coordinated Pickering emulsion catalyst (GO-DAP-$PdCl_2$) was developed in this study. It was prepared by immobilizing DAP onto graphene oxide. An amine ligand was grafted onto the graphene oxide surface through an epoxide ring-opening reaction, and $PdCl_2$ was subsequently coordinated to the material in the form of Pd^{II}. The resulting Pickering emulsion, stabilized by GO-DAP at the oil–water interface, exhibited uniform droplet distribution and high stability. The GO-DAP-$PdCl_2$ catalyst shows excellent catalytic activity for the Suzuki–Miyaura coupling reaction under a Pickering emulsion system, achieving 95% conversion within 3 h at 85 °C, with a turnover frequency as high as 14 100 h^{-1}. The catalyst maintained 85% of its activity after six consecutive runs and displayed broad substrate compatibility. The Pickering emulsion provided a large interfacial area for the biphasic reaction, which effectively reduced the mass-transfer resistance during the reaction. The amine-based ligand stabilized the active site through covalent bonding, which achieved the dual effects of reaction microenvironment optimization and active site protection.

Author contributions

M. Li, J. Huang and Y. Shan designed the research. Y. Shan and X.-B. Wang supervised the experimental work. M. Li and J. Huang performed most of the experiments and characterization analyses. M. Li wrote the original manuscript, and Y. Shan and X.-B. Wang revised the manuscript.

Conflicts of interest

There are no conflicts to declare.

Data availability

The data supporting this article have been included as part of the supplementary information (SI). Additional raw data can be obtained upon reasonable request from the corresponding author, Y. Y. Shan.

Supplementary information is available. See DOI: https://doi.org/10.1039/d5lf00367a.

Acknowledgements

The authors gratefully acknowledge financial support from the National Natural Science Foundation of China (Grant No. 22578308).

Notes and references

1 N. Miyaura, K. Yamada and A. Suzuki, A new stereospecific cross-coupling by the palladium-catalyzed reaction of 1-alkenylboranes with 1-alkenyl or 1-alkynyl halides, *Tetrahedron Lett.*, 1979, **20**(36), 3437–3440, DOI: 10.1016/s0040-4039(01)95429-2.

2 D. Han, Z. Zhang, Z. Bao, H. Xing and Q. Ren, Pd-Ni nanoparticles supported on titanium oxide as effective catalysts for Suzuki-Miyaura coupling reactions, *Front. Chem. Sci. Eng.*, 2017, **12**(1), 24–31, DOI: 10.1007/s11705-017-1669-4.

3 T. Niwa, Y. Uetake, M. Isoda, T. Takimoto, M. Nakaoka, D. Hashizume, H. Sakurai and T. Hosoya, Lewis acid-mediated Suzuki-Miyaura cross-coupling reaction, *Nat. Catal.*, 2021, **4**(12), 1080–1088, DOI: 10.1038/s41929-021-00719-6.

4 S. Akkoç, Importance of some factors on the Suzuki-Miyaura cross-coupling reaction, *J. Chin. Chem. Soc.*, 2021, **68**(6), 942–951, DOI: 10.1002/jccs.202000351.

5 M. C. D'Alterio, E. Casals-Cruanas, N. V. Tzouras, G. Talarico, S. P. Nolan and A. Poater, Mechanistic aspects of the palladium-catalyzed Suzuki-Miyaura cross-coupling reaction, *Chem. – Eur. J.*, 2021, **27**(54), 13481–13493, DOI: 10.1002/chem.202101880.

6 Y. Jiang, B. Xie and J. Zhang, Highly reactive and reusable heterogeneous activated carbons-based palladium catalysts for Suzuki-Miyaura reaction, *Chin. J. Chem. Eng.*, 2023, **60**, 165–172, DOI: 10.1016/j.cjche.2023.02.013.

7 S. D. Walker, T. E. Barder, J. R. Martinelli and S. L. Buchwald, A rationally designed universal catalyst for Suzuki-Miyaura coupling processes, *Angew. Chem., Int. Ed.*, 2004, **43**(14), 1871–1876, DOI: 10.1002/anie.200353615.

8 B. Bhattacharyya, A. J. Kalita, A. K. Guha and N. Gogoi, Phosphonate functionalized N-heterocyclic carbene Pd(II) complexes as efficient catalysts for Suzuki-Miyaura cross coupling reaction, *J. Organomet. Chem.*, 2021, **953**, 122067, DOI: 10.1016/j.jorganchem.2021.122067.

9 M. P. Crockett, A. S. Wong, B. Li and J. A. Byers, Rational design of an iron-based catalyst for Suzuki-Miyaura cross-couplings involving heteroaromatic boronic esters and tertiary alkyl electrophiles, *Angew. Chem., Int. Ed.*, 2020, **59**(13), 5392–5397, DOI: 10.1002/anie.201914315.

10 P. P. Mpungose, Z. P. Vundla, G. E. M. Maguire and H. B. Friedrich, The current status of heterogeneous palladium catalysed heck and Suzuki cross-coupling reactions, *Molecules*, 2018, **23**(7), 1676, DOI: 10.3390/molecules23071676.

11 D. E. Jose, U. S. Kanchana, T. V. Mathew and G. Anilkumar, Recent studies in Suzuki-Miyaura cross-coupling reactions with the aid of phase transfer catalysts, *J. Organomet. Chem.*, 2020, **927**, 121538, DOI: 10.1016/j.jorganchem.2020.121538.

12 G. Ding, L. Hao, H. Xu, L. Wang, J. Chen, T. Li, X. Tu and Q. Zhang, Atomically dispersed palladium catalyses Suzuki-Miyaura reactions under phosphine-free conditions, *Commun. Chem.*, 2020, **3**(1), 43, DOI: 10.1038/s42004-020-0289-y.

13 X. Yang, X. Li and Y. Huang, Single-atom catalysis: a promising avenue for precisely controlling reaction pathways, *Front. Chem. Sci. Eng.*, 2024, **18**(7), 79, DOI: 10.1007/s11705-024-2434-0.

14 M. D. Wodrich and X. Hu, Natural inspirations for metal-ligand cooperative catalysis, *Nat. Rev. Chem.*, 2017, **2**(1), 0099, DOI: 10.1038/s41570-017-0099.

15 A. Falconnet, M. Magre, B. Maity, L. Cavallo and M. Rueping, Asymmetric magnesium-catalyzed hydroboration by metal-ligand cooperative catalysis, *Angew. Chem., Int. Ed.*, 2019, **58**(49), 17567–17571, DOI: 10.1002/anie.201908012.

16 R. Mondal, A. K. Guin, G. Chakraborty and N. D. Paul, Metal-ligand cooperative approaches in homogeneous catalysis using transition metal complex catalysts of redox noninnocent ligands, *Org. Biomol. Chem.*, 2022, **20**, 296–328, DOI: 10.1039/d1ob01153g.

17 Y. Tang, Y. Han, J. Zhao, Y. Lv, C. Fan, L. Zheng, Z. Zhang, Z. Liu, C. Li and Y. Lin, A rational design of metal-organic framework nanozyme with high-performance copper active centers for alleviating chemical corneal burns, *Nano-Micro Lett.*, 2023, **15**(1), 112, DOI: 10.1007/s40820-023-01059-9.

18 Y. Wang, L. Zhu, Z. Shao, G. Li, Y. Lan and Q. Liu, Unmasking the ligand effect in manganese-catalyzed hydrogenation: mechanistic insight and catalytic application, *J. Am. Chem. Soc.*, 2019, **141**(43), 17337–17349, DOI: 10.1021/jacs.9b09038.

19 L. Y. Li and C. Hou, Mechanistic insight into the borrowing hydrogen reaction catalysed by a Pd MLC catalyst: Unveiling the ligand-to-ligand hydrogen transfer pathway, *Org. Chem. Front.*, 2024, **11**(14), 3997–4006, DOI: 10.1039/d4qo00688g.

20 M. R. Elsby and R. T. Baker, Strategies and mechanisms of metal-ligand cooperativity in first-row transition metal complex catalysts, *Chem. Soc. Rev.*, 2020, **49**(24), 8933–8987, DOI: 10.1039/d0cs00509f.

21 J. L. Obeso, M. T. Huxley, C. Leyva, J. Gabriel Flores, N. Martín-Guaregua, M. Viniegra, J. Aguilar-Pliego, J. Reyes, I. A. Ibarra and R. A. Peralta, The role of dynamic metal-ligand bonds in metal-organic framework chemistry, *Coord. Chem. Rev.*, 2023, **496**, 215403, DOI: 10.1016/j.ccr.2023.215403.

22 N. Davison, K. Zhou, P. G. Waddell, C. Wills, C. Dixon, S. X. Hu and E. Lu, Versatile coordination modes of multidentate neutral amine ligands with group 1 metal cations, *Inorg. Chem.*, 2022, **61**(8), 3674–3682, DOI: 10.1021/acs.inorgchem.1c03786.

23 H. Zu, Q. Li, R. Zhang, Z. Xiong, B. Li, J. Wang, R. Wang, Q. Fang and H. Yang, Amphiphilic covalent organic framework nanoparticles for Pickering emulsion catalysis with size selectivity, *Angew. Chem., Int. Ed.*, 2024, **63**(13), e202314650, DOI: 10.1002/anie.202314650.

24 H. Zou, H. Shi, S. Hao, Y. Hao, J. Yang, X. Tian and H. Yang, Boosting catalytic selectivity through a precise spatial control of catalysts at Pickering droplet interfaces, *J. Am. Chem. Soc.*, 2023, **145**(4), 2511–2522, DOI: 10.1021/jacs.2c12120.

25 D. Gonzalez Ortiz, C. Pochat-Bohatier, J. Cambedouzou, M. Bechelany and P. Miele, Current trends in Pickering emulsions: Particle morphology and applications, *Engineering*, 2020, **6**(4), 468–482, DOI: 10.1016/j.eng.2019.08.017.

26 B. Pang, H. Liu and K. Zhang, Recent progress on Pickering emulsions stabilized by polysaccharides-based micro/nano-particles, *Adv. Colloid Interface Sci.*, 2021, **296**, 102522, DOI: 10.1016/j.cis.2021.102522.

27 L. Yang, J. Ge, H. Wu, H. Guo, J. Shan and G. Zhang, Study on the Pickering emulsions stabilized by SiO_2 nanoparticles for enhanced oil recovery, *J. Surfactants Deterg.*, 2024, **28**(2), 225–238, DOI: 10.1002/jsde.12794.

28 M. C. Li, Y. Zhang, J. Sun, K. Lv, X. Huang, X. Meng, Z. Li, N. Song, D. Yang and C. Liu, Lignin nanoparticle-stabilized Pickering emulsion: Mechanism, influencing parameter, and emerging application, *Adv. Colloid Interface Sci.*, 2025, **341**, 103476, DOI: 10.1016/j.cis.2025.103476.

29 A. M. Bago Rodriguez and B. P. Binks, Capsules from Pickering emulsion templates, *Curr. Opin. Colloid Interface Sci.*, 2019, **44**, 107–129, DOI: 10.1016/j.cocis.2019.09.006.

30 M. Li, Q. Song, Y. Wang and B. Liu, Pickering emulsions with low interface coverage but enhanced stability for emulsion interface catalysis and SERS-based detection, *Nat. Commun.*, 2025, **16**(1), 2490, DOI: 10.1038/s41467-025-57914-3.

31 L. Ni, C. Yu, Q. Wei, D. Liu and J. Qiu, Pickering emulsion catalysis: Interfacial chemistry, catalyst design, challenges, and perspectives, *Angew. Chem., Int. Ed.*, 2022, **61**(30), e202115885, DOI: 10.1002/anie.202115885.

32 X. Gao, L. Hou, W. Yang, L. Dong and X. Ge, Lignin-based nanoparticles stabilized Pickering emulsion for enhanced catalytic hydrogenation, *Langmuir*, 2025, **41**(3), 1937–1947, DOI: 10.1021/acs.langmuir.4c04464.

33 J. Tang, B. Zhang, M. Zhang and H. Yang, Interfacial effects of catalysis in Pickering emulsions, *J. Phys. Chem. Lett.*, 2024, **15**(35), 8973–8983, DOI: 10.1021/acs.jpclett.4c01781.

34 D. Liu, W. Zhou, J. Wu and T. Huang, Fractal characterization of graphene oxide nanosheet, *Mater. Lett.*, 2018, **220**, 40–43, DOI: 10.1016/j.matlet.2018.02.134.

35 I. Bychko, A. Abakumov, O. Didenko, M. Chen, J. Tang and P. Strizhak, Differences in the structure and functionalities of graphene oxide and reduced graphene oxide obtained from graphite with various degrees of graphitization, *J. Phys. Chem. Solids*, 2022, **164**, 110614, DOI: 10.1016/j.jpcs.2022.110614.

36 V. A. Chernov, N. V. Kovalenko and S. V. Mytnichenko, The use of quasi-bragg diffuse scattering for express measurement of changes in multilayer d-spacing, *Nucl. Instrum. Methods Phys. Res., Sect. A*, 2001, **470**, 155–157, DOI: 10.1016/s0168-9002(01)01015-4.

37 D. López-Díaz, J. A. Delgado-Notario, V. Clericò, E. Diez, M. D. Merchán and M. M. Velázquez, Towards understanding the Raman spectrum of graphene oxide: The effect of the chemical composition, *Coatings*, 2020, **10**(6), 524, DOI: 10.3390/coatings10060524.

38 V. Thapliyal, M. E. Alabdulkarim, D. R. Whelan, B. Mainali and J. L. Maxwell, A concise review of the raman spectra of carbon allotropes, *Diamond Relat. Mater.*, 2022, **127**, 109180, DOI: 10.1016/j.diamond.2022.109180.

39 R. Arrigo, M. E. Schuster, Z. Xie, Y. Yi, G. Wowsnick, L. L. Sun, K. E. Hermann, M. Friedrich, P. Kast, M. Hävecker, A. Knop-Gericke and R. Schlögl, Nature of the N-Pd interaction in nitrogen-doped carbon nanotube catalysts, *ACS Catal.*, 2015, **5**(5), 2740–2753, DOI: 10.1021/acscatal.5b00094.

40 M. Tiwari, M. G. Basavaraj and V. R. Dugyala, Pickering emulsions: role of particle wettability and adhesive force on droplet bridging, *Langmuir*, 2024, **40**(50), 26474–26486, DOI: 10.1021/acs.langmuir.4c03241.

41 Z. Zhao, T. Wang, J. Yue, Y. Fan and Y. Wang, Highly efficient oil-fouling and foam removal achieved by surfactant mixed systems, *RSC Appl. Interfaces*, 2024, **1**, 173–182, DOI: 10.1039/D3LF00145H.

42 A. C. Braga, N. H. Morgon, G. Ujaque and F. Maseras, Computational characterization of the role of the base in the Suzuki-Miyaura cross-coupling reaction, *J. Am. Chem. Soc.*, 2005, **127**(25), 9298–9307, DOI: 10.1021/ja050583i.

43 R. T. Pinto, K. S. Feu, C. J. Dalmaschio, A. Nascimento and V. Lacerda, Oil recovery improvements based on pickering emulsions stabilized by cellulose nanoparticles and their underlying mechanisms: A Review, *ACS Omega*, 2025, **10**(4), 3262–3281, DOI: 10.1021/acsomega.4c08428.

44 N. Tangsuphoom and J. N. Coupland, Effect of heating and homogenization on the stability of coconut milk emulsions, *J. Food Sci.*, 2005, **70**(8), e466–e470, DOI: 10.1111/j.1365-2621.2005.tb11516.x.

45 E. Iranpoor, F. Panahi, F. Roozbin, S. Erfan and S. Rahimi, Palladium-catalyzed aminocarbonylation of aryl halides with 2,4,6-trichloro-1,3,5-triazine/formamide mixed reagent, *Eur. J. Org. Chem.*, 2016, **9**, 1781–1787, DOI: 10.1002/ejoc.201501607.

46 P. R. Melvin, A. Nova, D. Balcells, N. Hazari and M. Tilset, DFT investigation of Suzuki-Miyaura reactions with aryl sulfamates using a dialkylbiarylphosphine-ligated palladium catalyst, *Organometallics*, 2017, **36**(18), 3664–3675, DOI: 10.1021/acs.organomet.7b00642.

47 G. Sabharwal, K. C. Dwivedi, C. Das, T. R. K. Rana, A. Dutta, G. Rajaraman and M. S. Balakrishna, Detailed mechanistic studies on PNN-palladium pincer complex catalyzed Suzuki-Miyaura cross-coupling reaction proceeding through a $Pd^{II}/Pd^{III}/Pd^{IV}$ catalytic cycle, *J. Catal.*, 2024, **440**, 115825, DOI: 10.1016/j.jcat.2024.115825.

48 K. Masuda and S. Kobayashi, Direct and quantitative monitoring of catalytic organic reactions under heterogeneous conditions using direct analysis in real time mass spectrometry, *Chem. Sci.*, 2020, **11**(17), 4501–4506, DOI: 10.1039/d0sc00021c.

49 R. G. Nicholls, A. Jerfy and A. B. Roy, The determination of the initial velocity of enzyme-catalysed reactions, *Anal. Biochem.*, 1974, **61**(1), 93–100, DOI: 10.1016/0003-2697(74)90336-4.

50 D. Choudhury, B. Das, D. D. Sarma and C. N. R. Rao, XPS evidence for molecular charge-transfer doping of graphene, *Chem. Phys. Lett.*, 2010, **497**(1–3), 66–69, DOI: 10.1016/j.cplett.2010.07.089.

51 R. D. Feltham and P. Brant, XPS studies of core binding energies in transition metal complexes. 2. Ligand group shifts, *J. Am. Chem. Soc.*, 1982, **104**(3), 641–645, DOI: 10.1021/ja00391a001.

52 S. Jabeen, R. A. Khera, J. Iqbal and M. Asgher, Design, synthesis and application of triazole ligands in Suzuki-Miyaura cross coupling reaction of aryl chlorides, *J. Mol. Struct.*, 2020, **1206**, 127753, DOI: 10.1016/j.molstruc.2020.127753.

53 P. S. Gahlaut, D. Gautam, P. Lama and B. Jana, Unusual coordination of a 1,2,3-triazolyl-pyridine ligand in a Pd(ii) complex: application in the Suzuki-Miyaura coupling reaction, *New J. Chem.*, 2023, **47**(14), 6871–6879, DOI: 10.1039/d3nj00206c.

54 M. T. Chen and Z. L. Kao, Effect on orthometallation of NHC palladium complexes toward the catalytic activity studies in Suzuki coupling reaction, *Dalton Trans.*, 2017, **46**(47), 16394–16398, DOI: 10.1039/c7dt03280c.